JPE 16-4-10

http://dx.doi.org/10.6113/JPE.2016.16.4.1336
ISSN(Print): 1598-2092 / ISSN(Online): 2093-4718

An Equivalent Carrier-based Implementation of a Modified 24-Sector SVPWM Strategy for Asymmetrical Dual Stator Induction Machines

Kun Wang†, Xiaojie You*, and Chenchen Wang*

†,*School of Electrical Engineering, Beijing Jiaotong University, Beijing, China

Abstract

A modified space vector pulse width modulation (SVPWM) strategy based on vector space decomposition and its equivalent carrier-based PWM realization are proposed in this paper, which is suitable for six-phase asymmetrical dual stator induction machines (DSIMs). A DSIM is composed of two sets of symmetrical three-phase stator windings spatially shifted by 30 electrical degrees and a squirrel-cage type rotor. The proposed SVPWM technique can reduce torque ripples and suppress the harmonic currents flowing in the stator windings. Above all, the equivalent relationship between the proposed SVPWM technique and the carrier-based PWM technique has been demonstrated, which allows for easy implementation by a digital signal processor (DSP). Simulation and experimental results, carried out separately on a simulation system and a 3.0 kW DSIM prototype test bench, are presented and discussed.

Key words: Carrier-based PWM, Dual stator induction machine (DSIM), Space vector pulse width modulation (SVPWM), Vector space decomposition

I. INTRODUCTION

Nowadays, multiphase variable-speed drives are widely discussed used in various industrial applications and transportation systems such as electric/hybrid vehicles, traction locomotives, electric propulsion ships and aerospace applications [1], [2]. When compared with their standard three-phase counterparts, multiphase drives have several advantages [3], [4]; they make it easier to realize high-power levels using existing power switch devices, have lower torque ripple, less dc-link current harmonics, better torque production per ampere for the same machine volume, higher efficiency and reliability.

Among the different multiphase motor drive solutions, one of the most widely discussed is the two-level six-phase voltage source inverter (VSI) fed dual stator induction machine (DSIM), having two sets of three-phase symmetrical windings spatially shifted by 30 electrical degrees with isolated neutral points, as shown in Fig. 1. Over the years, various topics pertinent to this new type of motor drive system have been covered in depth in the literature, including machine modeling and optimal designing [5], [6], high-performance control strategies [7], [8], digital current controller designing [9], [10], harmonic current suppression [11], fault-tolerant operation [12] and various pulse width modulation (PWM) techniques [13]-[22].

In general, the existing research related to the PWM control of DSIMs has two main approaches. The most straightforward of these approaches is undoubtedly the utilization of carrier-based PWM methods [13]-[16]. Double zero-sequence injection (DZSI) techniques are extensions of the six-phase case of the three-phase zero-sequence injection techniques [23], [24]. They are simpler and easier to implement in digital systems [14], [15]. Space-vector PWM (SVPWM) techniques are probably the most popular methods. In [14], [15], two sets of conventional three-phase SVPWM, shifted by 30 electrical degrees, are applied to the two three-phase windings of a DSIM. Actually, these dual three-phase SVPWM methods are equivalent to the DZSI technique [14]. In addition, 12-sector SVPWM [17]-[21] and 24-sector SVPWM [22] are presented based on vector space decomposition [17], [18]. The 12-sector

Manuscript received Dec. 5, 2015; accepted Mar. 13, 2016
Recommended for publication by Associate Editor Jung-Ik Ha.
†Corresponding Author: 12117371@bjtu.edu.cn
Tel: +86-010-51684029, Beijing Jiaotong University
*School of Electrical Engineering, Beijing Jiaotong University, China

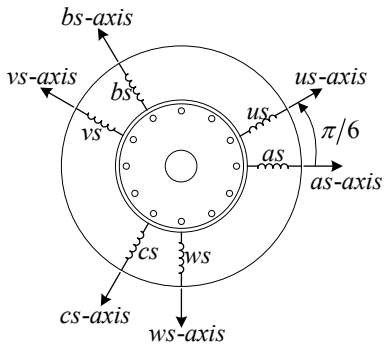

Fig. 1. Dual stator induction machine windings.

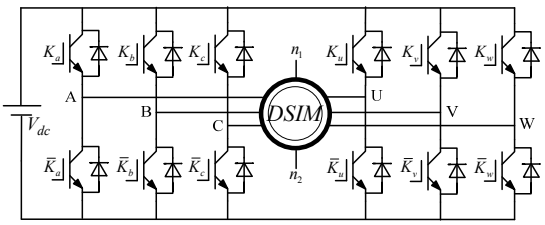

Fig. 2. Six-phase VSI fed DSIM.

SVPWM techniques produce asymmetrical waveforms and usually contain more than two transitions (from high to low or from low to high) per phase of the PWM waveforms within a sampling period, which increases the switching frequency of inverters and is difficult to achieve with digital implementation [22]. The 24-sector SVPWM techniques overcome these drawbacks of the 12-sector SVPWM and offer great advantages from the point of view of harmonic performance and the ease of digital implementation [22]. However, the algorithm is still complicated and requires high computational efforts [14].

In this paper, a modified 24-sector SVPWM technique is proposed and the correlation between this modified 24-sector SVPWM and the carrier-based PWM methods is also established. A comparative study of the harmonic flux analysis among the existing 24-sector SVPWM, modified 24-sector SVPWM and the DZSI techniques is developed and discussed. Simulation and experimental results are obtained from a software simulation system and a 3.0 kW prototype machine using a DSP control board.

II. Review of Modulation Techniques for DSIM

A DSIM drive system is shown in Fig. 2. The two three-phase stator windings are identical and symmetrical with to the two neutral points being isolated. They are fed by two sets of three-phase voltage source inverters (VSIs), which share the same DC link.

A. Double Zero-sequence Injection PWM Technique

The double zero-sequence injection (DZSI) approach has been introduced in [13]-[16], and is shown in Fig. 3. It is actually an extension to the six-phase case of the three-phase zero-sequence injection technique. The double zero-sequence voltages for the two three-phase windings are computed separately with a simple logic algorithm as given below.

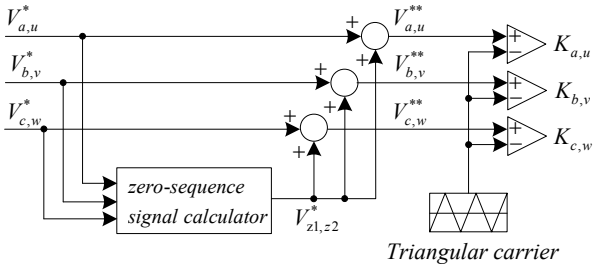

Fig. 3. Modulation scheme for double zero-sequence injection technique.

$$V^*_{z1} = -(V^*_{\max 1} + V^*_{\min 1})/2$$
$$V^*_{z2} = -(V^*_{\max 2} + V^*_{\min 2})/2 \quad (1)$$

where $V_{\max 1}{}^*$ and $V_{\min 1}{}^*$ represent the maximum and minimum values of the sinusoidal reference voltages $V_{a,b,c}{}^*$, while $V_{\max 2}{}^*$ and $V_{\min 2}{}^*$ represent the maximum and minimum values of the sinusoidal reference voltages $V_{u,v,w}{}^*$. The DZSI has an advantage in terms of being easily implemented without any computational effort, which is the reason it is widely used [13]-[16].

B. Existing 24-sector SVPWM Technique

There are a total of 64 switching states for a six-phase VSI, which determines 60 active voltage vectors and 4 zero voltage vectors. Each voltage vector is represented by a decimal number corresponding to a binary number ($K_wK_vK_uK_cK_bK_a$), which gives the states of the upper switches. Based on the vector space decomposition theory [17], [18], the inverter voltage vectors can be transformed into the (α-β), (x-y) and (o_1-o_2) subspaces. The electromechanical energy conversion variables are mapped in the (α-β) subspace, while the non-electromechanical energy conversion variables can be found in the other subspaces [18]. The zero sequence components in the (o_1-o_2) subspace can be omitted from consideration, since the two neutral points are isolated [18], [22].

According to the principles of the six-phase SVPWM techniques proposed in [17]-[19], four variables need to be controlled to make sure that the PWM waveforms can generate the maximum (α-β) and minimum (x-y) voltage amplitudes during each sampling period. Therefore, a set of four active voltage vectors and appropriate zero voltage vectors should be chosen to satisfy these two conditions at the same time.

The 24-sector SVPWM technique (SVPWM24), presented in [22], employs twelve large voltage vectors with maximum magnitudes, twenty four small ones with half magnitudes and zero voltage vectors (0,7,56,63) in the (α-β) subspace to

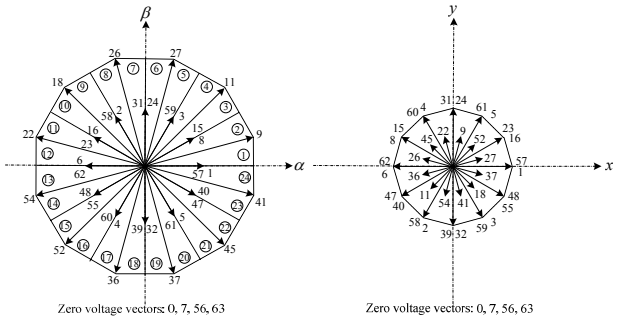

(a) (α-β) subspace. (b) (x-y) subspace.

Fig. 4. Presentation of the voltage vectors having maximum and half magnitude in (α-β) and (x-y) subspaces.

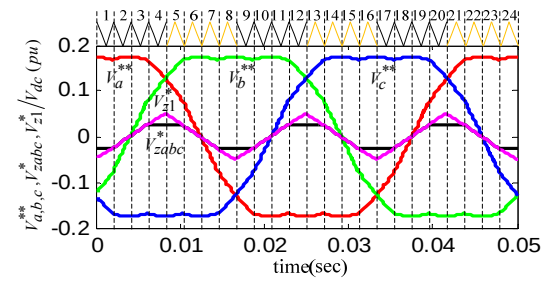

(a) winding *abc*.

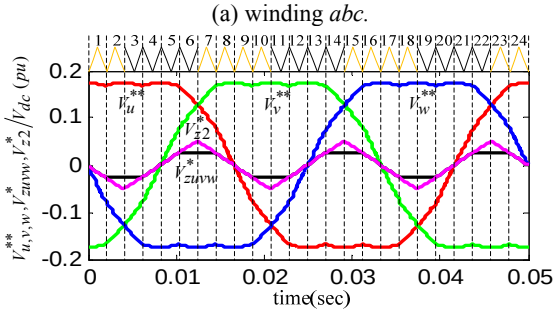

(b) winding *uvw*.

Fig. 5. Modulation voltages and zero sequence voltages of SVPWM24.

synthesize the reference voltage vectors. These active voltage vectors divide the (α-β) subspace into twenty four sectors, as shown in Fig. 4(a). For example, the reference voltage vector located in sector 1 is obtained by three large voltage vectors 41, 9, and 11 and one small voltage vector 15 in each sampling period.

The 24-sector SVPWM method offers greater advantages concerning the reduction of the low order harmonic components in the motor phase currents. However, the algorithm is very complicated and requires greater computational efforts [14], [22]. As shown in Fig. 5, the zero-sequence voltages V_{zabc}^* and V_{zuvw}^* of the SVPWM24 are not identical to the V_{z1}^* and V_{z2}^* of the DZSI, which means that the SVPWM24 is difficult to realize in the carrier-based PWM technique. Then a modified 24-sector SVPWM technique is proposed in this paper. It offers good output performance that is similar to that of the existing 24-sector SVPWM and can also be realized by an equivalent carrier-based PWM method.

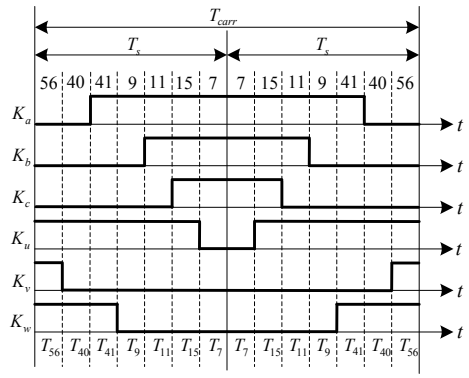

Fig. 6. Switching sequences of SVPWM24_M in sector 1.

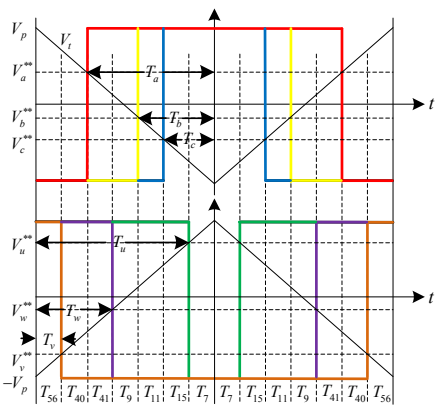

Fig. 7. Timing of gating pulses of carrier-based PWM equivalent to modified 24-sector SVPWM technique.

III. Proposed PWM Strategy for DSIMs

A. Modified 24-sector SVPWM Technique

In the modified 24-sector SVPWM technique (SVPWM24_M), three large active voltage vectors and two small active voltage vectors in the (α-β) subspace are used in each sampling period. For example, in the first sector three large vectors 41, 9, and 11; two small vectors 40 and 15; as well as two zero voltage vectors 56 and 7 are selected. In order to be realized in the carrier-based PWM method, an equal division of the duration times is applied to the two zero voltage vectors ($T_{56} = T_7$, in sector 1) and two small voltage vectors ($T_{40} = T_{15}$, in sector 1). The PWM waveforms in the first sector are given in Fig. 6.

B. Correlation between the Modified 24-sector SVPWM and the Carrier-Based PWM Techniques

Fig. 6 illustrates the switching sequence and duration times (T_{56}, T_{40}, T_{41}, T_9, T_{11}, T_{15}, T_7) of the voltage vectors in the first sector of the modified 24-sector SVPWM technique. The timing of the gating pulses of the carrier-based PWM equivalent to the SVPWM24_M is also presented in Fig. 7. Since the initial levels of the PWM waveforms in winding *abc* and winding *uvw* are opposite in the first sector, the equivalent triangular carrier waves are opposite as well. The durations T_a,

T_b and T_c of gating pulses for phases A, B and C are expressed as:

$$\begin{aligned} T_a &= T_7 + T_{15} + T_{11} + T_9 + T_{41} \\ T_b &= T_7 + T_{15} + T_{11} \\ T_c &= T_7 + T_{15} = 0.5(T_s - T_{41} - T_9 - T_{11}) \end{aligned} \tag{2}$$

In the modified 24-sector SVPWM technique, the duration times of the two small voltage vectors are equally distributed, as well as the two zero voltage vectors. In the first sector, they can be expressed as:

$$T_{40} = T_{15}, \ T_{56} = T_7 \tag{3}$$

In Fig.7, it is evident that during the applying times (T_{41}+ T_9) and T_{11}, the bus voltage V_{dc} is applied to the lines *ab* and *bc*, respectively [23]. Employing the principle of volt-seconds over the sampling period T_s, it is possible to obtain:

$$\begin{aligned} (T_{41} + T_9)V_{dc} &= (V_a^* - V_b^*)T_s \\ T_{11}V_{dc} &= (V_b^* - V_c^*)T_s \end{aligned} \tag{4}$$

where V_a^*, V_b^* and V_c^* ($V_{a,b,c}^*$ for short) are the phase voltages of the winding *abc*. Then the time intervals (T_{41}+T_9) and T_{11} can be obtained as:

$$\begin{aligned} T_{41} + T_9 &= (V_a^* - V_b^*)T_s / V_{dc} \\ T_{11} &= (V_b^* - V_c^*)T_s / V_{dc} \end{aligned} \tag{5}$$

To correlate the carrier-based method with the modified 24-sector SVPWM method, firstly a set of new input reference voltages $V_{a,b,c}^{**}$ and $V_{u,v,w}^{**}$ has to be found. The equation describing the triangle waveform of the winding *abc* in Fig. 7 is expressed as:

$$\frac{V_t + V_p}{2V_p} = \frac{t}{T_s} \tag{6}$$

where V_t and V_p=0.5V_{dc} represent the instantaneous and peak values of the triangle waveform, respectively. By introducing equations (3)-(5) into (6), a new reference voltage for phase A can be calculated as:

$$\begin{aligned} V_a^{**} &= 0.5V_{dc}\left(\frac{2}{T_s}T_a - 1\right) = \frac{V_{dc}}{2T_s}(T_{41} + T_9 + T_{11}) \\ &= \frac{(V_a^* - V_c^*)}{2} \end{aligned} \tag{7}$$

The difference between the new reference voltage V_a^{**} and the original reference voltage V_a^*, which is defined as the zero sequence voltage, is obtained as:

$$V_{z1a}^* = V_a^{**} - V_a^* = \frac{(V_a^* - V_c^*)}{2} - V_a^* = -\frac{(V_a^* + V_c^*)}{2} \tag{8}$$

The zero sequence voltages for phase B and phase C can be derived in the same way as above, and the results of the winding *abc* in the first sector are summarized below.

$$V_{z1\_sector1}^* = V_{z1a}^* = V_{z1b}^* = V_{z1c}^* = -(V_a^* + V_c^*)/2 \tag{9}$$

Extending the same procedure to all of the other sectors, the new reference voltages $V_{a,b,c}^{**}$ and the zero sequence voltage V_{z1}^* for the winding *abc* can be summarized as follows:

TABLE I
INITIAL LEVELS OF PWM WAVEFORMS IN EVERY SECTOR

Sector	1,2	3,4	5,6	7,8	9,10	11,12
Initial levels of ABC	Low	Low	High	High	Low	Low
Initial levels of UVW	High	Low	Low	High	High	Low
Sector	13,14	15,16	17,18	19,20	21,22	23,24
Initial levels of ABC	High	High	Low	Low	High	High
Initial levels of UVW	Low	High	High	Low	Low	High

$$\begin{aligned} V_{a,b,c}^{**} &= V_{a,b,c}^* + V_{z1}^* \\ V_{z1}^* &= -(V_{\max 1}^* + V_{\min 1}^*)/2 \end{aligned} \tag{10}$$

For the winding *uvw*, although the triangle waveform is opposite to that in the winding *abc*, shown in Fig. 7, similar results can be achieved as below:

$$\begin{aligned} V_{u,v,w}^{**} &= V_{u,v,w}^* + V_{z2}^* \\ V_{z2}^* &= -(V_{\max 2}^* + V_{\min 2}^*)/2 \end{aligned} \tag{11}$$

Since new reference voltages $V_{a,b,c}^{**}$ and $V_{u,v,w}^{**}$ have been obtained, one more factor must be considered. The modified 24-sector SVPWM technique divides the four zero voltage vectors into two sets: (56, 7) and (63, 0). In each sector, the switching sequence employs only one set of zero voltage vectors and they alternate every two sectors. As a result, the initial levels of the PWM waveforms change every two sectors as well. For example, the switching sequences in sector 1 and sector 2 use the zero voltage vectors 56 and 7, as shown in Fig. 6, the initial levels of the phases *abc* are 'low', which means the PWM waveforms are switching from low to high during the switching period. Meanwhile, the initial levels of the phases *uvw* are 'high', which means that the PWM waveforms are switching from high to low. The switching sequences in sector 3 and sector 4 employ the zero voltage vectors 63 and 0, the corresponding initial levels of the phases *abc* and *uvw* are both 'low'. The results for all of the sectors are summarized in Table I.

In order to obtain an equivalent effect from the SVPWM24_M, the triangular carrier waves for the two windings should be adjusted according to the initial levels of each sector, as in the case of sector 1 shown in Fig. 7. Therefore, the modified 24-sector SVPWM technique can be realized by the DZSI technique with the triangular carrier waves adjusted.

C. Realization of the Modified 24-sector SVPWM in the Equivalent Carrier-Based PWM Method

According to the analysis above, a new carrier-based PWM technique, which is equivalent to the modified 24-sector SVPWM, can be easily realized through the control scheme shown in Fig. 8. The modulation scheme contains two parts:

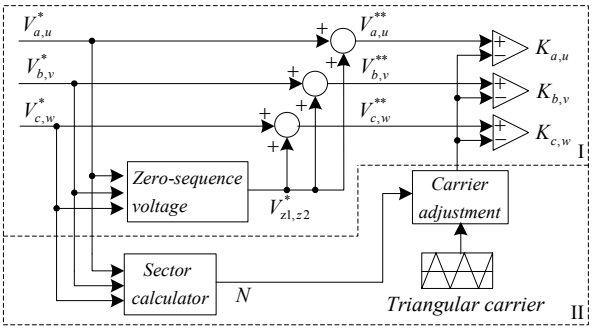

Fig. 8. Modulation scheme for new carrier-based PWM method.

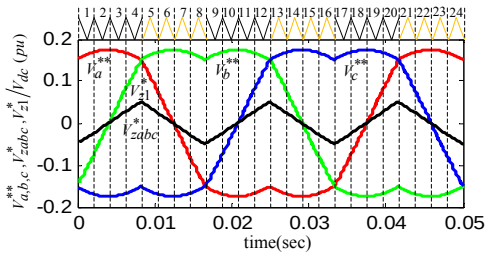

(a) winding *abc*.

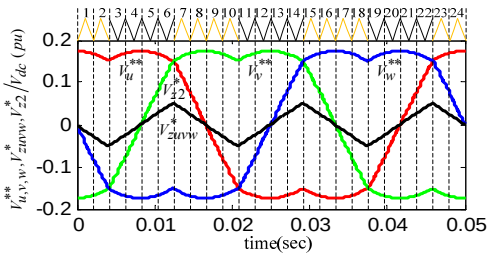

(b) winding *uvw*.

Fig. 9. Modulation voltages and zero sequence voltages of SVPWM24_M.

the first part is to obtain the modulation voltages by adding double zero sequence voltages to the reference sinusoidal voltages, which is exactly the same as the method of the existing DZSI [13]-[16]; the second part is to adjust the triangular carrier waves according to the initial levels in each sector.

The simulation waveforms of the modulation voltages $V_{a,b,c}^{**}$ and $V_{u,v,w}^{**}$ and the zero sequence voltages V_{z1}^{*} and V_{z2}^{*} are presented in Fig. 9. Compared with the DZSI, the new carrier-based PWM technique needs to adjust the triangular carrier waves according to the sector number. The triangular waves on the top of the figures represent the triangular carrier waves used in each sector. For example, in winding *abc*, the triangular carrier waves in black are used in sectors 1-4, 9-12 and 17-20. Meanwhile, the triangular carrier waves in yellow are used in sectors 5-8, 13-16 and 21-24. Therefore, the modified 24-sector SVPWM can be realized in an equivalent carrier-based PWM technique. As is well known, the carrier-based PWM technique is much simpler and easier in terms of calculation complexity and digital signal processor (DSP) implementation than its SVPWM counterpart.

IV. Waveform Quality

Since the switching frequency harmonics determine the torque ripple of a motor load, the line current total harmonic distortion (THD) of a line-connected VSI and so on, the output voltage waveform quality of a PWM-VSI drive is determined by the switching frequency harmonic characteristics [25]-[28]. It can be verified that the harmonic current and harmonic flux trajectories are only different in scale and that the harmonic flux requires no load information, which means it only characterizes the switching frequency behavior of a modulator [25]. From this perspective, harmonic flux is a pretty good evaluation index for comparing different modulation techniques.

A. Calculation of Normalized Per-Fundamental Cycle RMS Harmonic Flux Values

Unlike the situations in conventional three-phase machines [25], the harmonic flux in a DSIM is calculated in both the (α-β) and (x-y) subspaces [26]-[28]. The harmonic flux in the Nth carrier cycle, which is normalized to λ_b, is calculated as follows:

$$\lambda_b = 2V_{dc}T_s / \pi$$
$$\lambda_{h\alpha\beta}(M,\theta,t) = \frac{1}{\lambda_b}\int_{NT_s}^{(N+1)T_s}(V_{s\alpha\beta k} - V_{s\alpha\beta}^{*})dt \quad (12)$$
$$\lambda_{hxy}(M,\theta,t) = \frac{1}{\lambda_b}\int_{NT_s}^{(N+1)T_s}(V_{sxyk})dt$$

In the above formulas, $V_{s\alpha\beta k}$ and V_{sxyk} are the inverter output voltage vectors of the kth state in the (α-β) and (x-y) subspaces, respectively. The per-fundamental cycle rms value of the harmonic flux is the most important performance characteristic of a modulation technique because it determines the output waveform quality and harmonic losses of the inverter [25]. Because of symmetry, the per-fundamental cycle rms harmonic flux values in the (α-β) and (x-y) subspaces can be calculated in the following:

$$\lambda_{hfrms-\alpha\beta}^2(M) = \frac{12}{\pi}\int_0^{\pi/12}\lambda_{hrms-\alpha\beta}^2(M,\theta)d\theta$$
$$\lambda_{hfrms-xy}^2(M) = \frac{12}{\pi}\int_0^{\pi/12}\lambda_{hrms-xy}^2(M,\theta)d\theta \quad (13)$$

where:

$$\lambda_{hrms-\alpha\beta}^2(M,\theta) = \int_0^1\lambda_{h\alpha\beta}^2(M,\theta,t)dt$$
$$\lambda_{hrms-xy}^2(M,\theta) = \int_0^1\lambda_{hxy}^2(M,\theta,t)dt \quad (14)$$

In the above formulas, the variables $\lambda^2_{hrms-\alpha\beta}$ and $\lambda^2_{hrms-xy}$ are the per-carrier cycle rms values of the harmonic fluxes in the (α-β) and (x-y) subspaces, respectively. Nevertheless, the (x-y) current components are limited by the stator leakage inductance [22] and the introduction of the coefficient $k_{\alpha xy}=\sigma L_s/L_{lsxy}$ is necessary to evaluate and compare the performance of the PWM techniques. In the above formula, $\sigma=L_s-L_m^2/L_r$, L_s , L_r and L_m represent the stator leakage

inductance, rotor leakage inductance and mutual leakage inductance between stator and rotor in the (α-β) subspace. Meanwhile, L_{lsxy} is the transformed stator leakage inductance in the (x-y) subspace. Then the total per-fundamental cycle rms harmonic flux normalized to λ_b is calculated as follows:

$$\lambda_{hfrms}^2(M) = \lambda_{hfrms-\alpha\beta}^2(M) + k_{\sigma xy}^2 \lambda_{hfrms-xy}^2(M) \qquad (15)$$

The corresponding results for the SVPWM24 [22], SVPWM24_M and DZSI [15] techniques are calculated and summarized in the Appendix.

B. Performance Comparison

The curves of the normalized per-fundamental cycle rms harmonic flux for the SVPWM24, SVPWM24_M and DZSI techniques are plotted in Fig. 10. It is obvious that the rms value of the harmonic flux varies with respect to the PWM techniques. Compared with the SVPWM24 technique, the SVPWM24_M method proposed in this paper provides better harmonic characteristics. The curves in Fig. 10(a) show that the three PWM techniques offer similar performance in the low modulation index range, while in the high modulation index range, the DZSI exhibits the best performance in the (α-β) subspace. From the results shown in Fig. 10(b), the SVPWM24_M presents the best performance in the (x-y) subspace. According to [18], the harmonics of the order k=12n±1, (n=1,2,3…) are mapped in the (α-β) subspace, while the harmonics of the order k=6n±1, (n=1,3,5…) are transformed in the (x-y) subspace. That is to say, the low order harmonic components in the (x-y) subspace have a greater influence on the motor output performance. The results of the total rms harmonic flux are shown in Fig. 10(c), (d) and (e) with the coefficients $k_{\alpha xy}$ equal to 0.5, 1 and 2, respectively. When $k_{\alpha xy}$<1, as shown in Fig. 10(c), the DZSI technique presents the best harmonic characteristic. When $k_{\alpha xy}$=1, as shown in Fig. 10(d), the DZSI and SVPWM24_M techniques offer the same performances, which are better than those of the SVPWM24 technique. When $k_{\alpha xy}$>1, as shown in Fig. 10(e), the SVPWM24_M exhibits the best harmonic performance.

V. Simulation and Experimental Results

To verify the validity and feasibility of the modified 24-sector SVPWM technique, a simulation system and a 3.0 kW prototype DSIM test bench have been established. The DSIM prototype fed by two three-phase inverters sharing a common DC link, as shown in Fig. 2, is rewound from a conventional three-phase machine. The stator windings employ a type of single layer and diameter pitch, and the detailed motor parameters are listed in Table II.

Simulation and experimental results for the SVPWM24, SVPWM24_M and DZSI techniques under constant V/f control are presented in this paper. The average switching frequency for all of the PWM techniques is set to 2 kHz.

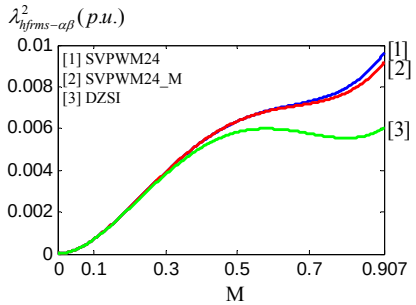

(a) (α-β) rms harmonic flux.

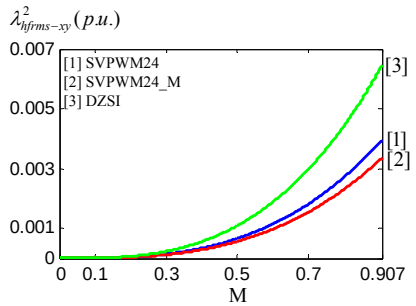

(b) (x-y) rms harmonic flux.

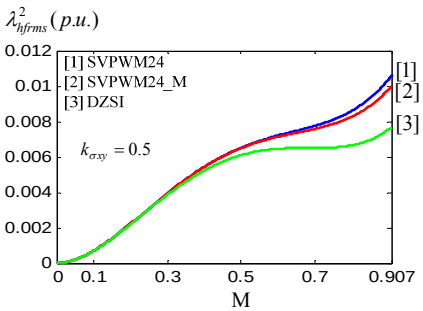

(c) Total rms harmonic flux ($k_{\alpha xy}$= 0.5).

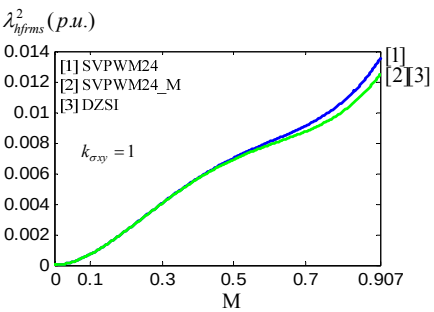

(d) Total rms harmonic flux ($k_{\alpha xy}$= 1).

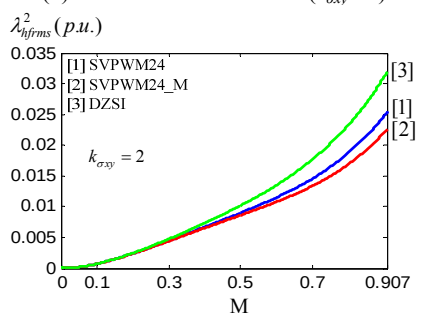

(e) Total rms harmonic flux ($k_{\alpha xy}$= 2).

Fig. 10. Normalized per-fundamental cycle rms harmonic flux values for SVPWM24, SVPWM24_M and DZSI techniques.

TABLE II
MOTOR SPECIFICATIONS

Meaning	Unit	Value
Rated power	kW	3.0
Rated phase voltage	V	110
Rated phase current	A	6.1
Rated frequency	Hz	50
No. of pole pairs	-	1
Stator resistance	Ω	0.723
Rotor resistance	Ω	0.815
Stator leakage inductance	mH	6.243
Rotor leakage inductance	mH	6.243
Stator leakage inductance in (*x*-*y*) subspace	mH	0.596

From the simulation results, it can be observed that the SVPWM24 and SVPWM24_M present similar good performance in the (*α*-*β*) and (*x*-*y*) subspaces. The DZSI technique offers an advantage in the (*α*-*β*) subspace. However, it has the worst performance in the (*x*-*y*) subspace, which agrees with the results shown in Fig. 10.

The experimental phase current waveforms and FFT analysis for all of the SVPWM techniques are given in Fig. 12 and Fig. 13. The motor operates at 20Hz and 40Hz, respectively. It needs to be noted that the DSIM prototype used in the experimental test bench was rewound from a traditional three-phase induction machine without much optimization. The experimental results can still show that the proposed SVPWM24_M technique has the smallest THD values and offers the best output current quality.

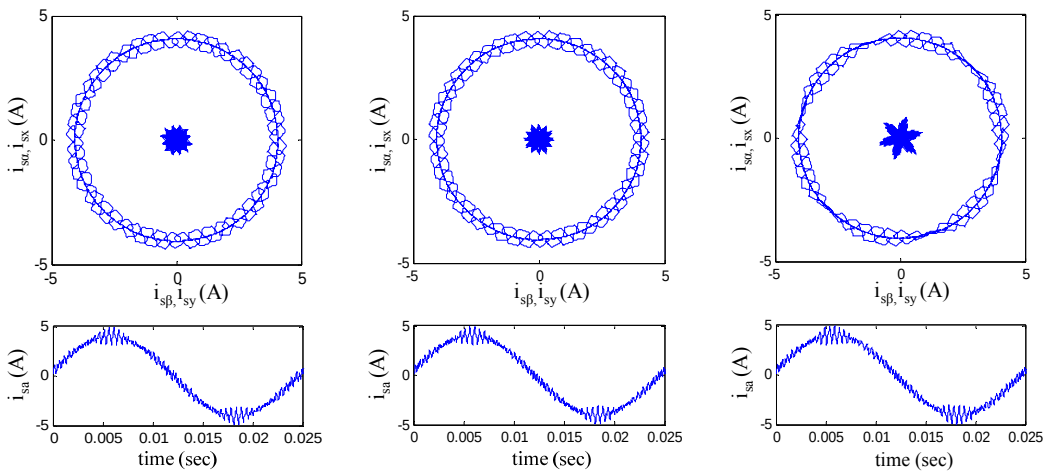

(a) SVPWM24. (b) SVPWM24_M. (c) DZSI.

Fig. 11. Simulation results of SVPWM24, SVPWM24_M and DZSI techniques with motor operating at 40Hz. From top to bottom: (*α*-*β*) and (*x*-*y*) subspace current trajectories, phase-A current.

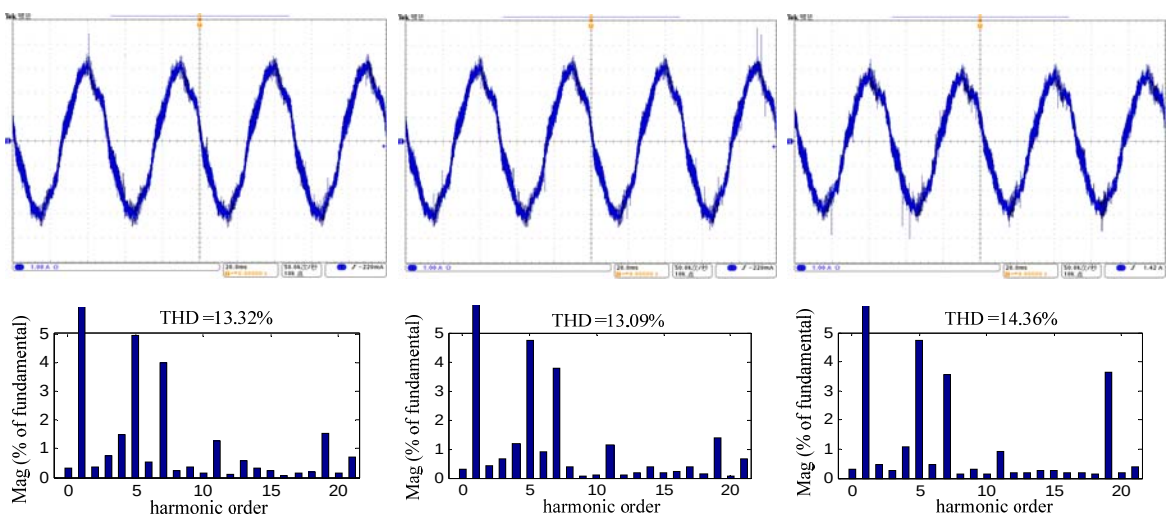

(a) SVPWM24. (b) SVPWM24_M. (c) DZSI.

Fig. 12. Experimental results of SVPWM24, SVPWM24_M and DZSI techniques with motor operating at 20Hz. From top to bottom: phase-A current and FFT analysis of phase-A current.

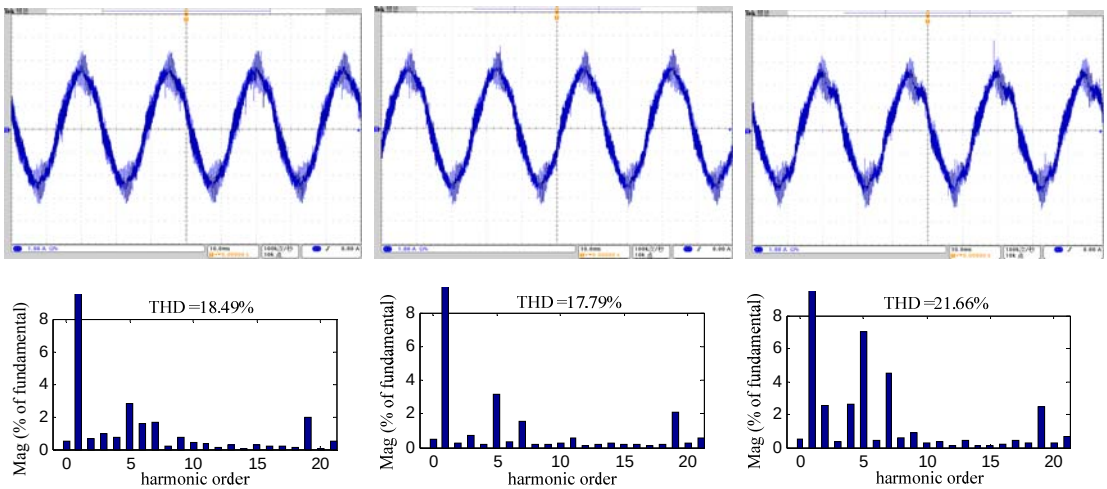

(a) SVPWM24. (b) SVPWM24_M. (c) DZSI.

Fig. 13. Experimental results of SVPWM24, SVPWM24_M and DZSI techniques with motor operating at 40Hz. From top to bottom: phase-A current and FFT analysis of phase-A current.

VI. CONCLUSION

In this paper, a modified 24-sector SVPWM (SVPWM24_M) technique based on the vector space decomposition theory has been presented. It is suitable for six-phase voltage source inverter fed dual stator induction machines. Compared with the existing 24-sector SVPWM technique, the proposed SVPWM24_M offers better harmonic characteristics in the whole voltage range. In addition, an equivalent relationship between the SVPWM24_M and the carrier-based PWM is also demonstrated in this paper, which means that the complexity of the digital implementation process can be greatly simplified. The validity of the discussion is verified by simulation and experimental results.

APPENDIX

The per-fundamental cycle rms normalized harmonic flux was calculated for all the discussed PWM techniques. The formulas are given below.

SVPWM24:

$$\begin{aligned}\lambda^2_{hfrms-\alpha\beta}(M) &= \frac{1}{12}M^2+\frac{1}{36\pi^2}(56\sqrt{3}+63\sqrt{6}-57\sqrt{2}-228)M^3\\ &\quad+\frac{1}{8\pi^3}(24\pi+27-21\sqrt{3}-8\sqrt{3}\pi)M^4\\ \lambda^2_{hfrms-xy}(M) &= \frac{1}{36\pi^2}(-63\sqrt{6}+228-88\sqrt{3}+57\sqrt{2})M^3\end{aligned} \tag{16}$$

SVPWM24_M:

$$\begin{aligned}\lambda^2_{hfrms-\alpha\beta}(M) &= \frac{1}{12}M^2+\frac{1}{72\pi^3}(-81\sqrt{3}+108\pi)M^4\\ &\quad+\frac{1}{72\pi^2}(-249-60\sqrt{2}+76\sqrt{3}+36\sqrt{6})M^3\\ \lambda^2_{hfrms-xy}(M) &= \frac{1}{72\pi^2}(249+60\sqrt{2}-140\sqrt{3}-36\sqrt{6})M^3\end{aligned} \tag{17}$$

DZSI:

$$\begin{aligned}\lambda^2_{hfrms-\alpha\beta}(M) &= \frac{1}{12}M^2+\frac{1}{72\pi^2}(36-126\sqrt{2}+40\sqrt{3}-18\sqrt{6})M^3\\ &\quad+\frac{1}{72\pi^3}(-81\sqrt{3}+108\pi)M^4\\ \lambda^2_{hfrms-xy}(M) &= \frac{1}{72\pi^2}(-36+126\sqrt{2}-104\sqrt{3}+18\sqrt{6})M^3\end{aligned} \tag{18}$$

ACKNOWLEDGMENT

This work was supported by National Natural Science Foundation of China (No. 51507009) and the Fundamental Research Funds for the Central Universities (No. 2016YJS142).

REFERENCES

[1] E. Levi, R. Bojoi, F. Profumo, H. A. Toliyat, and S. Williamson, "Multiphase induction motor drives-a technology status review," *IET Electric Power Applications*, Vol. 1, No. 4, pp. 489–516, Jul. 2007.

[2] E. Levi, "Multiphase electric machines for variable-speed applications," *IEEE Trans. Ind. Electron.*, Vol. 55, No. 5, pp. 1893–1909, May 2008.

[3] M. A. Abbas, R. Christen, and T. M. Jahns, "Six-phase voltage source inverter driven induction motor," *IEEE Trans. Ind. Appl.*, Vol. IA-20, No. 5, pp. 1251–1259, Sep. 1984.

[4] R. H. Nelson and P. C. Krause, "Induction machine analysis for arbitrary displacement between multiple winding sets," *IEEE Trans. Power App. Syst.*, Vol. PAS-93, No. 3, pp. 841–848, May 1974.

[5] L. Xu and L. Ye, "Analysis of a novel stator winding structure minimizing harmonic current and torque ripple for dual six-step converter-fed high power AC machines," *IEEE Trans. Ind. Appl.*, Vol. 31, No. 1, pp. 84–90, Jan./Feb. 1995.

[6] D. Hadiouche, H. Razik, and A. Rezzoug, "On the modeling and design of dual-stator windings to minimize circulating harmonic currents for VSI fed AC machines," *IEEE Trans. Ind. Appl.*, Vol. 40, No. 2, pp. 506–515, Mar./Apr. 2004.

[7] G. K. Singh, K. Nam, and S. K. Lim, "A simple indirect field-oriented control scheme for multiphase induction machine," *IEEE Trans. Ind. Electron.*, Vol. 52, No. 4, pp. 1177–1184, Aug. 2005.
[8] M. Moghadasian, R. Kianinezhad, F. Betin, and G. A. Capolino, "Torque ripple minimization in direct torque control of six-phase induction machines using fuzzy inference systems," in *International Conference on Electrical Machines (ICEM)*, pp. 1–6, Sep. 2010.
[9] R. Bojoi, E. Levi, F. Farina, A. Tenconi, and F. Profumo, "Dual three-phase induction motor drive with digital current control in the stationary reference frame," *IEE Proceedings - Electric Power Applications*, Vol. 153, No. 1, pp. 129–139, Jan. 2006.
[10] F. Barrero, M. R. Arahal, R. Gregor, S. Toral, and M. J. Duran, "A proof of concept study of predictive current control for VSI-driven asymmetrical dual three-phase AC machines," *IEEE Trans. Ind. Electron.*, Vol. 56, No. 6, pp. 1937–1954, Jun. 2009.
[11] H. S. Che, E. Levi, M. Jones, W. P. Hew, and N. A. Rahim, "Current control methods for an asymmetrical six-phase induction motor drive," *IEEE Trans. Power Electron.*, Vol. 29, No. 1, pp. 407–417, Jan. 2014.
[12] D. Casadei, M. Mengoni, G. Serra, A. Tani, and L. Zarri, "Optimal fault-tolerant control strategy for multi-phase motor drives under an open circuit phase fault condition," in *18th International Conference on Electrical Machines (ICEM)*, pp. 1–6, Sep. 2008.
[13] F. Patkar and M. Jones, "Performance of an asymmetrical six-phase induction machine in single-and two-Neutral point configurations," in *48th International Universities' Power Engineering Conference (UPEC)*, pp. 1–6, Sep. 2013.
[14] R. Bojoi, A. Tenconi, F. Profumo, G. Griva, and D. Martinello, "Complete analysis and comparative study of digital modulation techniques for dual three-phase AC motor drives," in *IEEE 33rd Annual Power Electronics Specialists Conference (PESC)*, Vol. 2, pp. 851–857, 2002.
[15] J. Prieto, E. Levi, F. Barrero, and S. Toral, "Output current ripple analysis for asymmetrical six-phase drives using double zero-sequence injection PWM," in *37th Annual Conference on IEEE Industrial Electronics Society(IECON)*, pp. 3692–3697, Nov. 2011.
[16] A. Boglietti, R. Bojoi, A. Cavagnino, and A. Tenconi, "Efficiency analysis of PWM inverter fed three-phase and dual three-phase high frequency induction machines for low/medium power applications," *IEEE Trans. Ind. Electron.*, Vol. 55, No. 5, pp. 2015–2023, May 2008.
[17] K. Gopakumar, V. T. Ranganathan, and S. R. Bhat, "Split-phase induction motor operation from PWM voltage source inverter," *IEEE Trans. Ind. Appl.*, Vol. 29, No. 5, pp. 927–932, Sep./Oct. 1993.
[18] Y. Zhao and T. A. Lipo, "Space vector PWM control of dual three-phase induction machine using vector space decomposition," *IEEE Trans. Ind. Appl.*, Vol. 31, No. 5, pp. 1100–1109, Sep./Oct. 1995.
[19] D. Hadiouche, L. Baghli, and A. Rezzoug, "Space vector PWM techniques for dual three-phase AC machine: Analysis, performance evaluation, and DSP implementation," *IEEE Trans. Ind. Appl.*, Vol. 42, No. 4, pp. 1112–1122, Jul./Aug. 2006.
[20] K. Marouani, L. Baghli, D. Hadiouche, A. Kheloui, and A. Rezzoug, "Discontinuous SVPWM techniques for double star induction motor drive control," in *32nd Annual Conference on IEEE Industrial Electronics (IECON)*, pp. 902–907, Nov. 2006.
[21] D. Yazdani, S. A. Khajehoddin, A. Bakhshai, and G. Joos, "Full utilization of the inverter in split-phase drives by means of a dual three-phase space vector classification algorithm," *IEEE Trans. Ind. Electron.*, Vol. 56, No. 1, pp. 120–129, Jan. 2009.
[22] K. Marouani, L. Baghli, D. Hadiouche, A. Kheloui, and A. Rezzoug, "A new PWM strategy based on a 24–sector vector space decomposition for a six–phase VSI–fed dual stator induction motor," *IEEE Trans. Ind. Electron.*, Vol. 55, No. 5, pp. 1910–1920, May 2008.
[23] V. Blasko, "Analysis of a hybrid PWM based on modified space-vector and triangle-comparison methods," *IEEE Trans. Ind. Appl.*, Vol. 33, No. 3, pp. 756-764, May/Jun. 1997.
[24] S. R. Bowes and Y. S. Lai, "The relationship between space-vector modulation and regular-sampled PWM," *IEEE Trans. Ind. Electron.*, Vol. 44, No. 5, pp. 670–678, Oct. 1997.
[25] A. M. Hava, R. J. Kerkman, and T. A. Lipo, "Simple analytical and graphical methods for carrier-based PWM-VSI drives," *IEEE Trans. Power Electron.*, Vol. 14, No. 1, pp. 49–61, Jan. 1999.
[26] D. Dujic, M. Jones, and E. Levi, "Analysis of output current ripple rms in multi–phase drives using polygon approach," *IEEE Trans. Power Electron.*, Vol. 25, No. 7, pp. 1838–1849, Jul. 2010.
[27] D. Dujic, M. Jones, E. Levi, J. Prieto, and F. Barrero, "Switching ripple characteristics of space vector PWM schemes for five–phase two–level voltage source inverters-Part 1: Flux harmonic distortion factors," *IEEE Trans. Ind. Electron.*, Vol. 58, No. 7, pp. 2789–2798, Jul. 2011.
[28] M. Jones, D. Dujic, E. Levi, J. Prieto, and F. Barrero, "Switching ripple characteristics of space vector PWM schemes for five–phase two–level voltage source inverters – Part 2: Current ripple," *IEEE Trans. Ind. Electron.*, Vol. 58, No. 7, pp. 2799–2808, Jul. 2011.

Kun Wang was born in Hebei Province, China, in 1989. He received his B.S. degree in Electrical Engineering from Beijing Union University, Beijing, China, in 2011. He is presently working towards his Ph.D. degree in Electrical Engineering at Beijing Jiaotong University, Beijing, China. His current research interests includes multiphase machine control.

Xiaojie You was born in Fujian Province, China, in 1964. He received his M.S. degree in Electrical Engineering from the China Agricultural University, Beijing, China, in 1989; and his Ph.D. from the Czech Technical University, Prague, Czech Republic, in 2001. From 2002 to 2004, he was a Post-doctoral Research Fellow at Tsinghua University, Beijing, China. From 2004 to 2006, he was an Associate Professor in the School of Electrical Engineering, Beijing Jiaotong University, where he has been a Professor and the Director of Power Electronic Research Institute, since 2006. His current research interests include AC drive electric locomotive control, switching power control, active power filters and power quality control.

Chenchen Wang was born in Anhui Province, China, in 1981. He received his B.S. and Ph.D. degrees in Electrical Engineering from Tsinghua University, Beijing, China, in 2003 and 2008, respectively. He is presently working as an Associate Professor in the School of Electrical Engineering, Beijing Jiaotong University, Beijing, China. His current research interests include motor control and multilevel converters.